Simultaneous source imaging by amplitude encoding

Jeff Godwin & Paul Sava
Center for Wave Phenomena, Colorado School of Mines

ABSTRACT
The computational cost of conventional shot-record imaging is large for today's wide-azimuth seismic surveys. One strategy to reduce the overall cost of seismic imaging is to migrate with multiple shot-gathers at once, a technique which is known as blended source imaging. Blended source imaging trades the reduced cost of imaging with the presence of artifacts (cross-talk) in the image. A special case of blended source imaging is that of zero phase-delay, or simultaneous sources. We show that a theoretical framework using a matrix representation of the imaging process adequately describes both conventional and simultaneous source imaging. Furthermore, the matrix representation predicts both the quantity and strength of cross-talk artifacts prior to imaging, thus allowing us to decide a priori the trade off between cross-talk and speed. By exploiting our theoretical framework, we are able to design a simultaneous source encoding scheme, referred to as Truncated Singular Vector encoding (TSV), that trades a significantly reduced cost of imaging with spatial resolution. The TSV encoding allows us to reduce the cost of imaging by at least an order of magnitude relative to conventional shot-record migration. Overall, we provide a framework for finding simultaneous source encoding schemes, that produce good quality images at lower computational cost.

Key words: seismic imaging, migration, blended sources, simultaneous sources, singular value decomposition, shot-encoding, wave-equation, matrix representation.

1 INTRODUCTION

Today's seismic imaging challenges include imaging areas with increasingly complex geology, such as salt domes and overthrust regions. The major issues for imaging these areas are poor data quality and lack of seismic illumination, as the complex geology severely deforms seismic wavefields. One approach to resolving these issues is to obtain large amounts of redundant information from various acquisition directions via wide-azimuth or full-azimuth seismic surveys (Ting & Zhao, 2009). However, wide-azimuth surveys require significantly more time to acquire and even greater amounts to process. Subsequently, the cost of acquiring and processing a wide-azimuth survey is significantly more expensive than the cost of a conventional survey. Additionally, the cost of imaging in complex geology is much greater, because advanced wave-equation imaging algorithms such as reverse-time migration must be used. Therefore, both the financial and computational cost of today's large surveys is increasing at a rapid pace.

However, recent technological advances may reduce the cost of data acquisition and imaging for large seismic surveys. One of these technologies is acquisition using simultaneous or delayed sources (Womack, 1990; Beasley, 2008; Berkhout et al., 2008; Hampson et al., 2008; Blacquiere et al., 2009). As the name implies, simultaneous sources are multiple sources triggered at the same time but at different spatial locations. By acquiring multiple sources in a shot-gather, it is hoped that the amount of time that a survey requires reduces thus decreasing the acquisition costs. The downside to simultaneous source acquisition, is that simultaneous source data creates additional noise in the final seismic image. Presently, this issue is circumvented by deblending the simultaneous source shot-gathers to create separate shot-gathers for each source prior to imaging (Akerberg et al., 2008; Hampson et al., 2008; Spitz et al., 2008; Huo et al., 2009; Kim et al., 2009). The separated shot-gathers are then imaged using a conventional shot-record migration. The drawback to separating the shots is twofold. First, the sources must be separable, which typically implies that they are relatively isolated from one another in space which limits the maximum amount of shots that can be used at once during acquisition. Second, the imaging process is not sped up by separating the shots.

An alternative approach, is to reduce the cost of imaging by using multiple sources at once during imaging. This process, known as blended imaging, combines multiple shot-gathers together prior to migration, which reduces the number of migrations that are needed to produce a final image (Liu, 1999; Morton, 1999; Romero et al., 2000; Soubaras, 2006; Zhang et al., 2007; Berkhout et al., 2009; Perrone & Sava, 2009). Certain forms of blended imaging, such as plane-wave migration, are used in industry today, but many forms of blending (i.e. random phase) are not used today because they introduce a significant amount of noise to the image. However, the presence of the noise may be justified if the cost advantage over conventional shot-record migration is sufficiently high.

In conventional seismic imaging (shot-record migration), seismic data corresponding to individual shots are backpropagated independently to construct the receiver-wavefields. Concurrently, the source-wavefield for each shot is constructed by forward propagating the source using a known velocity model. An imaging condition is then applied to the individual reconstructed source and receiver wavefields to produce an image of the subsurface. Because this process is repeated for each shot, the cost of shot-record migration (SRM) is expressed as

$$C_s^t = N_s C_s, \tag{1}$$

where C_s^t is the total cost in computation time, N_s is the number of shot records, and C_s is the computational cost for each shot (Zhang et al., 2007). Since modern seismic surveys often consist of many tens of thousands of shots, and each shot may image a large area (a few km^2), the overall computational cost for seismic imaging is tremendous.

However, equation 1 hints at two possibilities to reduce the overall cost of imaging:

- reduce the cost of migrating each shot (i.e. reduce C_s), or
- reduce the number of shot-records used for migration (i.e. reduce N_s).

In most scenarios, reducing the cost of migrating each shot C_s is the most practical approach to reducing the cost of imaging because one can choose the algorithm that is used for wavefield reconstruction (i.e. wavefield extrapolation or reverse-time migration). However, much of today's imaging is done in areas with complex geology, so computationally expensive algorithms like reverse-time migration have to be used to produce accurate images. Therefore, most reductions in computational cost typically come from advances in computer hardware. In most cases however, our ability to create more demanding algorithms i.e. full anisotropic reverse-time migration, and acquire more data greatly exceeds the rate of hardware advances.

Furthermore, reducing the number of shots N_s that are used to image is not typically considered because both the signal-to-noise ratio and the illumination of the seismic image are negatively impacted by removing sources. An alternative to reducing the number of sources is to linearly combine multiple independent shot-records together into blended shot-records prior to migration (Romero et al., 2000). By doing so, we effectively reduce the number of migrations that are necessary from N_s to N_e, where N_e is the number of blended experiments. The ultimate goal of blended imaging is to image using all shots in a single migration. Therefore, the total cost of imaging using a blended migration scheme becomes:

$$C_e^t = N_e C_e. \tag{2}$$

Here, C_e^t is the total cost for a blended source migration, C_e is the cost of an individual blended record migration, which we assume to be the same as the SRM cost C_s. In practice, $C_e > C_s$ as blended shots must be migrated over larger aperture ranges (Romero et al., 2000). In general, as the number of blended experiments N_e decreases the overall cost of imaging decreases. In most instances, the reduction in cost by blending greatly outweighs the additional cost of extending the migration aperture as $N_e \ll N_s$, whereas C_e is only *somewhat* greater than C_s.

The blending process usually applies a phase delay to each shot-record and then linearly combines *all* of the shot records together into a series of blended experiments prior to migration (Morton, 1999; Liu, 1999; Romero et al., 2000; Soubaras, 2006; Zhang et al., 2007; Berkhout et al., 2009; Perrone & Sava, 2009). A single blended experiment may also be referred to as a realization. A combination of experiments or realizations, where the combination method may change from experiment to experiment, is referred to as a shot-encoding scheme. During the imaging process, both the encoded source- and receiver-wavefields are reconstructed. The conventional cross-correlation imaging condition is applied to the blended wavefields as follows,

$$R(\mathbf{x}) = \sum_e \sum_t \left(\sum_i W_s^i(\mathbf{x},t) \right) \left(\sum_j W_r^j(\mathbf{x},t) \right), \tag{3}$$

where i and j are the shot-record indices, $W_s{}^i(\mathbf{x},t)$ is the i^{th} reconstructed source wavefield, $W_r{}^j(\mathbf{x},t)$ is the j^{th} reconstructed receiver wavefield, e represents the blended shot-gathers index, t represents time and $\mathbf{x}$ is a vector of locations in space. When $i = j$, equation 3 computes the correlation of wavefields related to a single shot gather. Conversely, when $i \neq j$, equation 3 computes the value of the source and receiver wavefields that are not physically related to one another, hence these terms are referred to as cross-talk. In blended imaging, the cross-talk exists between each source and every other receiver wavefields and vice versa which means that the blended images are contaminated by a significant amount of cross-talk noise. Additionally, cross-talk is unlike most other noise in that it is: coherent, strong (amplitude), and virtually indistinguishable from geology (Romero et al., 2000). Therefore, cross-talk must be removed before an image is usable for interpretation.

Previous attempts to remove cross-talk from blended-images focused on modifying the phase-encoding scheme to introduce inconsistency between unrelated wavefields in order to decrease the contribution of the cross-talk terms (Morton, 1999; Liu, 1999; Romero et al., 2000; Zhang et al., 2007; Berkhout et al., 2009; Perrone & Sava, 2009). In these encoding schemes, multiple realizations of all or some of the shot-gathers are used to create images. Some common phase-encoding schemes include: planar (Liu, 1999), random

(Romero et al., 2000), harmonic (Zhang et al., 2007), and planar with dithering (Perrone & Sava, 2009) . Another shot-encoding option is to modulate the amplitude of the wavefields to reduce the contribution of cross-talk terms to the image (Soubaras, 2006). Regardless of encoding choice, the standard method to attenuate cross-talk in images from separate realizations of blended shots is conventional stacking.

A special case of blended source imaging is simultaneous source imaging, i.e. linearly combining shot-gathers with zero phase- and time-delay. The major advantage of simultaneous source imaging compared to blended imaging is that simultaneous source data can be acquired using the same recording time length, whereas blended source acquisition requires long recording times due to time-delays between sources. Thus, simultaneous source imaging reduces both the cost of conventional acquisition and the data volume (Beasley, 2008; Hampson et al., 2008). However, the same problems with cross-talk in blended source imaging plague simultaneous source imaging as well. To some extent, the cross-talk problem is worse in simultaneous source imaging as it is more difficult to create incoherency in the wavefields during imaging (Romero et al., 2000). Ultimately though, we want to image using simultaneous source data because this saves time in imaging and in acquisition.

This paper focuses on the intersection of using simultaneous sources for data acquisition as well as for imaging. We examine simultaneous source shot-encoding schemes that can be used to reduce the amount of cross-talk present in simultaneous source images. To reduce the cross-talk, we develop a theoretical framework that allows us to evaluate the relative amount of cross-talk produced by an encoding scheme. By exploiting the framework, we are able to design an encoding scheme that minimizes the cross-talk in the image. We illustrate our method on both a simple synthetic model and the Sigsbee salt-model. Overall, the primary goal of this paper is to reduce the cost of imaging by an *order of magnitude* by using simultaneous sources in the imaging process. The long-term goal (beyond this research) is to design a simultaneous source acquisition scheme so that both the cost of data acquisition and the cost of imaging are reduced by an order of magnitude.

2 SIMULTANEOUS SOURCE ENCODINGS

An optimal shot-encoding scheme minimizes the amount of cross-talk present in the migrated images after stacking together images from multiple simultaneous source experiments (Romero et al., 2000). There are two issues that must be addressed when using simultaneous encodings. First, spatially close simultaneous sources form partial plane-waves during the migration process, which reduces the spatial resolution of the migration. Second, the wavefields from sources that are spatially distant from one another may interfere during the imaging condition, producing cross-talk noise which reduces the signal-to-noise ratio of the final image. Therefore, simultaneous source encoding schemes must be carefully designed to minimize the negative effects of both of these issues.

2. 1 Matrix representation of wave-equation migration

To design simultaneous source encoding schemes, we could start by randomly selecting possible encodings schemes. However, this search spans a space that is infinitely large, and there is no guarantee that one would ever find an optimal encoding. Rather, we find that conventional seismic imaging can be described by a series of matrix operations, which can be expanded to include simultaneous source imaging. The matrix representation allows us to determine the overall suitability of a simultaneous shot-encoding scheme by determining the amount of cross-talk in the migrated image in advance.

Conventional shot-record migration is composed of two steps: wavefield reconstruction and the application of an imaging condition:

$$R(\mathbf{x}) = \sum_t \sum_e W_s^e(\mathbf{x},t) W_r^e(\mathbf{x},t). \tag{4}$$

For each shot gather, the source-and receiver-wavefields are reconstructed separately. Then, the two wavefields are cross-correlated together and summed over time or frequency, depending on the domain, to form a partial image. All of the partial images are then stacked together to form the final image. Mathematically, each source and receiver-wavefield can be thought to be an element in a vector that holds all source- or receiver-wavefields respectively,

$$\mathbf{W}_S = \left[W_S^1, W_S^2, ..., W_S^i, ..., W_S^{N_s}\right], \tag{5}$$

$$\mathbf{W}_R = \left[W_R^1, W_R^2, ..., W_R^i, ..., W_R^{N_s}\right], \tag{6}$$

where W_S and W_R are row vectors, N_s is the number of shot-gathers, composed of the back projected wavefields, W_S^i and W_R^i, respectively. The i^{th} elements of both W_S and W_R correspond to the same physical shot-gather. Thus, conventional seismic imaging is equivalent to the inner product of the two vectors,

$$R = W_S W_R^T, \tag{7}$$

where R is the constructed image, and the multiplication of two elements of the matrix is actually the application of the imaging condition between those wavefields. As indicated earlier, the application of the imaging condition implies a summation over either time or frequency depending on which domain we use for wavefield reconstruction. The summation over elements implies stacking the partial images together, Figure 1(a).

In order to expand this notation to simultaneous source imaging, we introduce an additional matrix, which we call the encoding matrix E. The encoding matrix is an $N_s \times N_e$ matrix, where N_e is the number of experiments and N_s is the number of shots in the survey. Each column in the encoding matrix corresponds to a single simultaneous source experiment, while each row acts as a weight for a particular wavefield. Thus, each column in the encoding matrix weighs all wavefields to determine how to combine them together prior to imaging. The weights may be fractional, positive or negative numbers, or may be binary numbers to indicate which wavefields to use or not use in an experiment. Figure 2(a) depicts a sample encoding matrix

(a) (b)

Figure 1. Conventional seismic imaging comprises wavefield reconstruction and the application of an imaging condition to produce an image for each shot-gather. If each wavefield is considered to be a component of a vector of source $\mathbf{W}_S$ or receiver $\mathbf{W}_R$ wavefields, then the imaging process is equivalent to the dot product of the W_S and W_R vectors (a). In the vector notation, an identity matrix (b) indicates that each source-wavefield is paired only with its corresponding receiver wavefield.

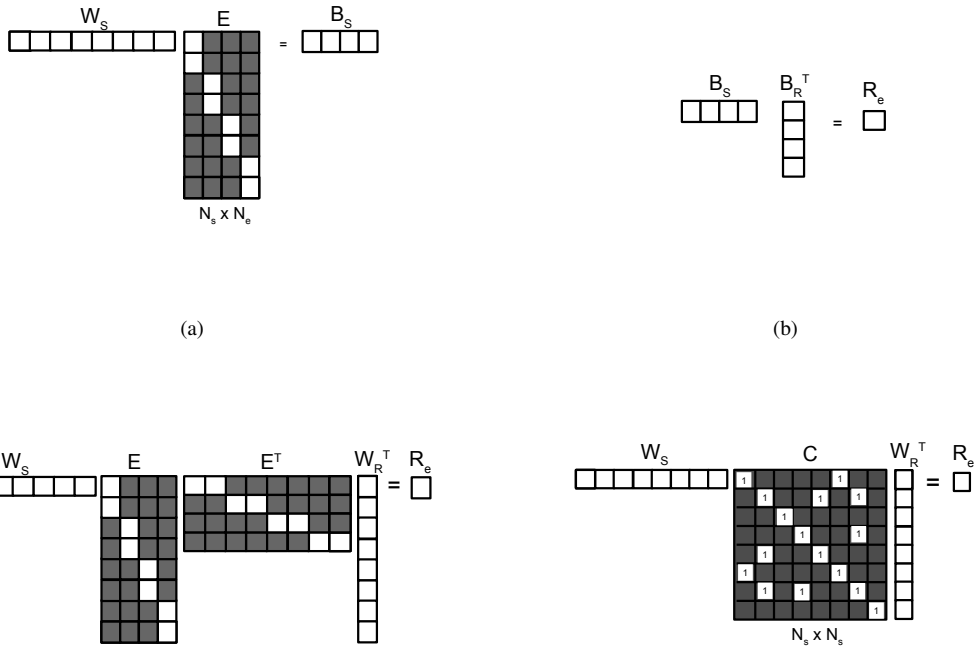

(a) (b)

(c) (d)

Figure 2. In contrast to conventional imaging, a simultaneous source encoding (a) uses an encoding matrix E to determine how to combine the source-wavefields together into a smaller vector $\mathbf{B_S}$ of blended wavefields. By analog, simultaneous source imaging (b) is the dot product of the $\mathbf{B_S}$ and $\mathbf{B_R}^T$ vectors. An overview of simultaneous source imaging (c) finds that the process is similar to conventional shot imaging, but with the presence of the encoding matrices. The R_e image is the original image plus additional artifacts from the cross-talk. By multiplying EE^T the cross-talk matrix C (d) is formed. The off-diagonal terms are the cross-talk artifacts that contaminate R_e.

where the weights are binary which selects only some wavefields per experiment.

The encoding matrix reduces the effective number of reconstructed wavefields that are used for imaging as follows:

$$B = WE, then \begin{cases} B_S &= W_S E \\ B_R &= W_R E \end{cases} \quad (8)$$

where WE is the projection of the wavefield vector (i.e W_S or W_R) onto the encoding matrix E, and B is the blended wavefield vector for the source- or receiver-wavefields (i.e. $B_S$or B_R). Therefore, B_S is the $1 \times N_e$ row vector of combined source-wavefields and B_R is an $N_e \times 1$ column vector of combined receiver-wavefields. Because the migration operator is linear, we can perform the combination of the source- and receiver-data, the product of WE, prior to wavefield reconstruction, thus reducing the necessary number of migrations from N_s to N_e. The final simultaneous source image R_e is represented by

$$R_e = B_S B_R^T, \quad (9)$$

and is shown in Figure 2(b). By substituting the expressions for B_S and B_R from equation 8 into equation 9, we obtain

$$R_e = W_S E E^T W_R^T, \quad (10)$$

which is similar to equation 7 and is illustrated in Figure 2(c). We refer to the product EE^T as the cross-talk matrix C, which is square and has dimensions of $N_s \times N_s$. Thus, equation 10 can be written as

$$R_e = W_S C W_R^T. \quad (11)$$

The cross-talk matrix C is similar to the identity I, but with additional off-diagonal terms as shown in Figure 2(d). This is a convenient description because equation 7 can be rewritten to include the identity matrix I to represent the pairing of each source wavefield with its corresponding receiver wavefield as

$$R = W_S I W_R^T. \quad (12)$$

Thus, the C matrix represents the formation of the conventional seismic image (i.e the diagonal terms) plus additional terms in the off-diagonals representing the pairing of wavefields that are not physically related to one another. Subsequently, the off-diagonal components of the C matrix are the cross-talk terms that we generate by using a certain encoding matrix E.

By examining equations 11 and 12, we find that the problem of designing optimal simultaneous source encodings becomes the problem of finding a cross-talk matrix C that is as close to the identity matrix I as possible in order to minimize the cross-talk in the image R_e. Consequently, the process of choosing a simultaneous source encoding becomes one of determining an encoding matrix E such that EE^T has the fewest off-diagonal components, or $EE^T \approx I$. In fact, if an encoding exists such that $EE^T = I$, then we can produce the same image as shot-record migration, at a cost proportional to the number of simultaneous source experiments N_e, instead of N_s. We note that the matrix representation in equation 11 is a more generic expression of the amplitude encoding scheme that Soubaras (2006) previously discussed.

2. 2 Identity matrix decompositions

The question of how to create an optimal simultaneous source encoding then becomes a question of how to decompose the identity matrix into a set of *rectangular* matrices E such that $EE^T \approx I$. In mathematics, a well-known decomposition of the identity matrix into two matrices is through the construction of an orthonormal basis.

For reference, a matrix Q is defined to be an orthonormal basis if $Q^T Q = I$ and $QQ^T = I$. Thus, we can reconstruct the identity matrix I from EE^T, if we use an orthonormal basis for our encoding matrix E. Unfortunately, orthonormal bases are represented by square matrices of the same size as that of the parent matrix or the same size as C which is $N_s \times N_s$ in our case. Therefore, an orthonormal basis encoding matrix provides no cost advantage compared to standard shot-record imaging.

While it may not be possible to directly use an orthonormal basis for an encoding matrix, one option is to truncate the columns of the orthonormal basis to form an encoding matrix that provides a substantial cost reduction. The truncated matrix's rows are no longer linearly independent, and hence no longer completely orthogonal to one another but, they still retain some of their original orthogonality. Soubaras (2006) arrived at a similar idea using a discrete Fourier basis for his experiments. The key in this scheme is to truncate the encoding matrix (orthonormal basis) such that the missing information degrades the image quality only slightly.

A logical choice for an orthonormal basis to use for an encoding matrix is to use the identity matrix itself. To do so, we would truncate columns starting from the end of the identity matrix I to form the encoding matrix E such that it is $N_s \times N_e$. However, truncating the identity matrix to form the encoding matrix removes entire shot-gathers from the reconstructed EE^T matrix which is not optimal because all of the shots should be used for imaging. Therefore only encoding matrices (truncated orthonormal bases) that use all of the shots are viable for consideration as encoding matrices.

2. 3 Data compression

The question then becomes which orthonormal basis should be used for the encoding matrix, and how best to truncate this matrix. This problem is well studied in other fields such as data compression (Rabbani, 1991; Salomon, 2007). In particular, the concept of projecting the wavefields onto an orthonormal basis and truncating the resulting matrix is directly similar to a class of *lossy* data compression algorithms referred to as transform algorithms (Rabbani, 1991; Salomon, 2007). Some common orthonormal bases used in transform compression include: Fourier, wavelet, and the discrete cosine. The key difference between the bases is the level of compression at a certain level of truncation and the quality of the recovered data at a specific level of compression. Along the same lines, Singular Value Decomposition (SVD) can be used to form orthonormal bases to compress data (Eckart & Young, 1936). In all cases, data are *irreversibly* lost once the orthonormal basis is truncated. In the context of the imaging problem, the loss of data

due to compression corresponds to a loss of information in the image, but the compression of the imaging process results in a decrease in the computational cost.

2. 4 Singular value decomposition

Due to data loss, it is impossible to reconstruct the identity matrix from the product of EE^T. An alternate way of approaching the problem is to design the cross-talk matrix C in advance so that it is close to the I matrix, and then decompose the C matrix into two matrices E and E^T. The benefit is that we control how close the approximation C is to the I matrix. In this way, the problem can be reformulated as an inverse problem. The problem of approximating a matrix by decomposition has been extensively studied in mathematics, and the optimal solution is given by the Singular Value Decomposition (SVD) (Eckart & Young, 1936).

In SVD, the matrix A is approximated by,

$$A = U\sigma V^T, \tag{13}$$

where A is an $M \times N$ matrix, U is $M \times N$, σ is an $N \times N$ diagonal matrix corresponding to the singular values, and V^T is $N \times N$. Both the columns of U and V^T form separate orthonormal bases, referred to as the left-singular and right-singular vectors respectively. In the special case where A is a real-valued, square, and symmetric matrix, which is the case for all cross-talk matrices C, then $U = V$ and equation 13 becomes

$$C = U\sigma U^T. \tag{14}$$

This expression is similar to $C = EE^T$ except that in equation 14 U is a square matrix and that σ is present. Thus, we are able to conclude that $E \approx U_{tc}$, where U_{tc} is the truncated matrix U. In order to formalize the relationship between the encoding matrix E and the singular vectors U, we truncate the columns of U (singular vectors) according to SVD theory, which indicates that we should keep the first N_e columns corresponding to the largest singular values. Additionally, we split the singular value matrix σ by taking the square root of the matrix and multiplying it to U_{tc}. Therefore, E and E^T are respectively:

$$E = U_{tc}\sqrt{\sigma_{tc}}, \tag{15}$$

$$E^T = \sqrt{\sigma^{tc}}U_{tc}^T. \tag{16}$$

We refer to the constructed encoding matrix E as the Truncated Singular Vector (TSV) encoding. For SVD, there exists an optimal truncation level for which most of the information in the decomposed matrix is preserved. This point can be identified using the singular values. Large singular values indicate which singular vectors contribute most to the reconstruction of the matrix C. Conversely, small singular values (close to zero) indicate that a singular vector does not have a significant contribution to the reconstruction of C. We note, that the product of EE^T is an *approximation* to C, as a result of truncating U, which in turn is an *approximation* of the identity matrix I, by design. Also, it should be noted that the E matrix from the SVD uses *all* sources, for each simultaneous source experiment.

2. 5 Constructing the cross-talk matrix

The construction of the C matrix to approximate I using SVD is of paramount importance to the quality of the final image R_e. Since the C matrix should be as close to the identity matrix as possible, there are at least a few clear choices. The first is to band the diagonal in the C matrix, such that there are upper and lower diagonals. This is equivalent to applying a boxcar filter to the I matrix, as in Figure 3(a). For the boxcar filter, the full window width is defined as $a = 2\sqrt{3}\sigma$, where a is the window width and σ is the standard deviation. Another option is to use a Gaussian filter, to gradually taper the values away from the diagonal in the approximating matrix as in Figure 3(b). The Gaussian filter is defined as the normal distribution with a mean μ and a standard deviation σ. In both cases, the additional components along the diagonal represent the construction of small plane-waves because this is equivalent to combining the images for spatially closest sources into the output image, which results in loss of spatial resolution. If the product of EE^T is close to the I matrix though, the loss in spatial resolution can be negligible.

There are many other options for possible C matrices, and this is by no means a comprehensive discussion. Our examples demonstrate how SVD can be used to approximate the Gaussian and boxcar diagonal matrices, and to reconstruct images that are very close to the image obtained by shot-record migration. We leave for future research the problem of determining the optimal approximation to the identity matrix.

3 EXAMPLES

We conduct a series of examples to illustrate the ability of the SVD to construct encodings for simultaneous source imaging on two models. The first model consists of point diffractors, which illustrates that our encoding schemes do not suffer from a significant loss of spatial resolution. The second model is the Sigsbee2A salt model which demonstrates the ability of the SVD to handle complex velocity models while maintaining spatial resolution. For each model, the SVD is performed for both the boxcar and Gaussian approximations to the identity matrix, Figures 3(a) and 3(b). The orthonormal matrix U is truncated to form the encoding matrix E based on the chosen number of experiments to perform N_e. The shot-gathers and source-wavelets are combined and weighted linearly according to the encoding matrix E prior to wavefield reconstruction. The combined data are then reconstructed using downward continuation, and the imaging condition is applied, which creates a partial image for an experiment. All of the partial images are stacked to form the final image. For each experiment, the theoretical speed up is given by the ratio:

$$K = \frac{N_s}{N_e} \tag{17}$$

where N_s is the number of sources available, and N_e is the number of experiments using for imaging. The ratio K represents how many times faster the encoded migration is compared to conventional shot record migration.

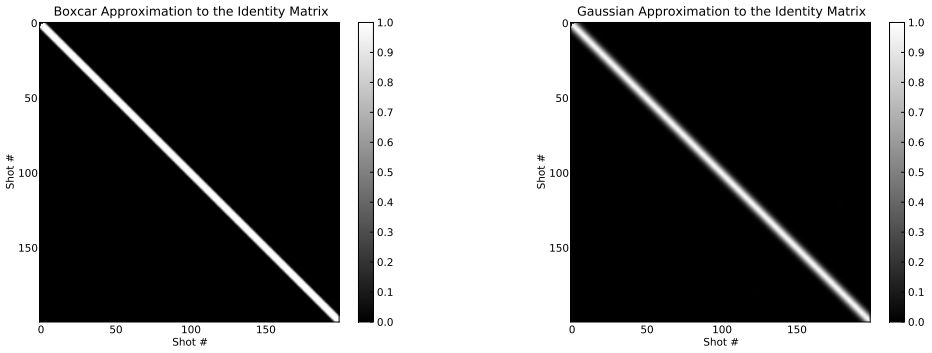

(a) (b)

Figure 3. The boxcar approximation of the identity matrix (b) with a boxcar window width a of 7, corresponding to a standard deviation σ of 2. The Gaussian approximation of the identity matrix (c) with $\mu = 0, \sigma = 2$. The only difference between (a) and (b) is the distribution (i.e. boxcar or Gaussian) used to band the identity matrix.

For each example, we show the encoding matrix E^T, the cross-talk matrix C, and a measure of relative amplitude. The measure of relative amplitude is given by

$$A_s = \sum_c |E_{s,c}|, \tag{18}$$

where A_s is the relative amplitude, c is the column index in the encoding matrix, s is the shot index in the encoding matrix, and E is the encoding matrix. The relative amplitude A_s is then normalized by the maximum value and measures the total effective contribution from each shot based on the weights in the encoding matrix. Ideally, this measure would be 1.0 for each shot, indicating that each shot's total contribution across all encodings is the same as its contribution for conventional shot-record migration. A less ideal condition is that all of the shots have contributions that are approximately 1.0. The relative contribution for each shot can exceed 1.0 because the singular values weight these terms. In this case, the amplitude of the conventional image can be reconstructed by performing a global rescaling. If the amplitude A_s varies as a function of shot, then the simultaneous source image contains spatial amplitude variability, which is a result of the simultaneous source encoding. The spatial variability in the amplitude causes certain portions of the image to be washed out and amplifies other portions of the image.

All the images are compared against one another and are clipped to the same relative range. This allows a direct comparison of amplitudes in the images, even though the amplitudes are not the same for the simultaneous experiments and for the conventional images. By doing so, we assume that the amplitudes in the simultaneous source experiments are erroneous by a constant scaling factor.

3. 1 Model with uniformly distributed point scatterers

The simple model is composed of a constant velocity, isotropic medium with 20 evenly spaced point diffractors arranged in a grid. We simulate 200 shots with receivers distributed over the full aperture of the model. Thus, there is no computational gain by decomposing the migration domain to represent limited aperture for each individual shot. For each simultaneous source experiment, the source wavelets and data are combined together into synthetic source and receiver datasets. The combined source- and receiver-wavefields are reconstructed using downward continuation. The standard cross-correlation imaging condition is applied to the reconstructed wavefields for each experiment to produce a partial image. The simultaneous source partial images are stacked together to form the final image. A conventional shot-record migration using downward continuation for all 200 shots is presented independently in Figure 4. This image serves as the benchmark for the simultaneous source images.

3. 1.1 Boxcar Approximation

The boxcar approximation to the identity matrix uses a window width a of 7, which corresponds to a standard deviation σ of 2. The first boxcar experiment involves 10 simultaneous source experiments which provides a speed-up K of 20. The singular values for the decomposition are shown in Figure 5. For reference, an interesting number of singular values to truncate is 50, where there is an abrupt change in the singular values. We truncate below this point because we are primarily interested in reducing the cost of imaging. Figures 6(a) and 6(b) shows the construction of the encoding matrix and the reconstruction of the C matrix using SVD for the boxcar approximation matrix for 10 simultaneous source experiments respectively. Figure 6(c) shows the amplitudes as a function of shot, which are spatially variable for 10 experiments. The encoding matrix, cross-talk matrix and amplitude variation for 20 experiments is shown in Figures 7(a), 7(b) and 7(c). Additionally, Figures 8(a), 8(b), and 8(c) show the encoding matrix E, the cross-talk matrix C and the amplitudes for 50 experiments.

The final image for 10 encodings using the boxcar approximation is shown in Figure 9(a). Figure 9(b) shows the

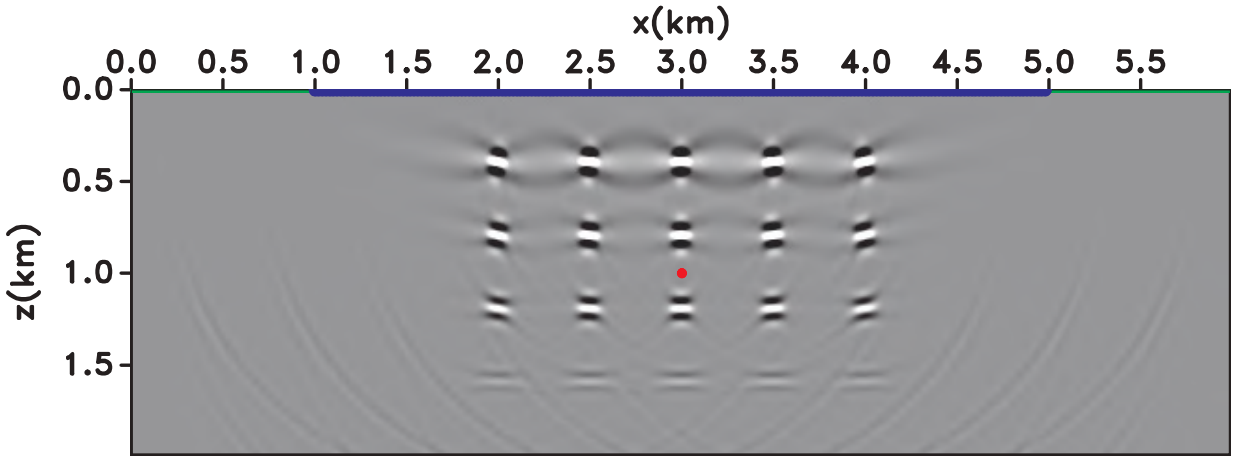

Figure 4. The stacked image for the point scatterer model using conventional shot-record migration for 200 shots.

image for 20 experiments, which results in a ratio K of 10. Figure 9(c) shows the final image for 50 experiments, which has a speed-up K of 4. Clearly, as the number of simultaneous experiments increases, the quality of the image increases. In the limit, the imaging would approximate the image for shot-record-migration, since the reconstructed cross-talk matrix approaches C which is close to the identity matrix.

3. 1.2 Gaussian Approximation

Another set of experiments demonstrates how the Gaussian approximation to the identity matrix I affects the final image. For the Gaussian approximation, the distribution is created with a mean $\mu = 0$ and standard deviation of $\sigma = 2$. The singular values in Figure 10 have smoother variation when compared to the boxcar approximation as in Figure 5 because the Gaussian approximation tapers off slowly instead of having an abrupt change in the cross-talk matrix. This implies that there are not abrupt changes in the simultaneous source image quality by including certain singular values or excluding some. Also, the singular values taper to zero rather quickly, indicating that the encodings corresponding to the zero singular values do not contribute to the image. Thus, the best possible image for the Gaussian approximation can be obtained by using all the singular values that are not zero or approximately the first 70 singular values. Figures 11(a), 11(b) and 11(c) show the encoding matrix, the cross-talk matrix and the amplitudes as a function of space for 10 experiments. The encoding matrix, cross-talk matrix and amplitude variation for 20 experiments are shown in Figures 12(a), 12(b) and 12(c). For the Gaussian approximation, we use truncate at 60 singular values because this seems to correspond to most of the information. Figures 13(a), 13(b) and 13(c) show the encoding matrix, cross-talk matrix and the amplitudes for 60 experiments ($K \approx 3$). The amplitudes are uniform across all shots, which indicates that the relative amplitude is not as spatially variable as for the other examples. Figure 14(a) shows the final image for 10 experiments, which has a speed-up factor K of 20. The image for 20 experiments has a K of 10, Figure 14(b). Figure 14(c) shows the final image for 60 experiments. This image is significantly closer to the target image than the images obtained from the other experiments.

3. 2 Sigsbee2A model

A similar group of experiments is conducted for the Sigsbee2A salt model. In this case, we create a new Sigsbee2A survey using 3200 shots to represent a shot at every possible shot location. Each shot is forward modelled using a finite-difference acoustic algorithm for the *full* aperture available in the Sigsbee model. In other words, the receivers are at every possible grid location on the surface. As in the simple model, there is no computational gain by decomposing the migration domain based on migration aperture, because the shots are simulated with receivers everywhere on the surface. For reference, the migration of all 3200 shots via conventional shot-record migration is shown in Figure 15. We construct the singular values for both the boxcar and Gaussian approximations, Figure 16(a) and 16(b). We evaluate only the Gaussian approximation to the identity matrix for the Sigsbee model because the singular values for the Gaussian approximation quickly taper to zero.

Figure 17(a) shows the image for 10 experiments using the Gaussian approximation. Theoretically, the image in Figure 17(a) is created *320 times* faster than the conventional image, but there is additional overhead in terms of disk usage that slows down the process. For comparison, Figure 17(b) shows the result from the Gaussian approximation for 30 experiments. The image quality is substantially improved for the 30 experiment image, compared to the 10 experiment image. For example, the 30 experiment image is less noisy in the salt body than the 10 experiment image. Additionally, the 30 experiment image is substantially clearer underneath the salt body ($x = 15.0km$, $4.5km < z < 8.0km$). Figure 17(c) shows the result from a Gaussian approximation using 100 experiments.

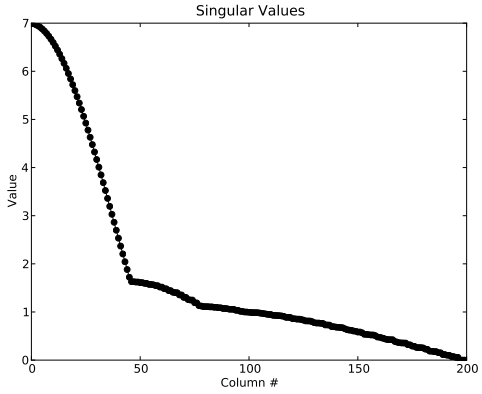

Figure 5. The singular values for the boxcar approximation to the identity matrix for the model with point scatterers. There is an abrupt change in slope of the singular values near $N_e = 50$, which seems to be an optimal point to truncate the singular values at. The singular values gradually taper to zero, indicating that all singular values contribute to the image, although the smaller singular values contribute less than large ones.

This image is created $32\times$ faster than that of the conventional migration. Figure 17(c) is of much better quality than both of the other experiments, and is visually close to Figure 15.

4 DISCUSSION

Our theoretical model has allowed the creation of an optimal simultaneous source encoding scheme that we refer to as the Truncated Singular Vector encoding (TSV). Our experiments confirm that the TSV encoding scheme produces nearly optimal migrated images, as the images are close to the conventionally migrated images with $C_e^t \ll C_s^t$. The main difference between the conventional image and the encoded image is that the amplitude of the encoded image changes spatially depending on the number of encodings used for imaging. Furthermore, the TSV encoding is able to reduce the cost of seismic imaging, by at least an order of magnitude. For the Sigsbee data set, the cost of seismic imaging is reduced by up to *100 times* for 3200 shots. We note that 3200 shots is excessive sampling for imaging Sigsbee and that a good quality image can be obtained using only 500 shots. Regardless, the TSV encoding is equally valid for 3200 shots or 500 shots, although the actual speed-up factor might be different.

In practice, some of the relative speed advantage K gained by using the TSV encoding is offset by the requirement of additional data input and output to produce the encoded experiments. If the combination procedure is efficiently spread over multiple machines with many disks, then this additional cost is negligible. However, the reduced cost comes at the expense of cross-talk noise and a spatial variation of the amplitudes in the image. The spatial amplitude variation is the result of an uneven weighting of shot-gathers by the encoding matrix. A possible way to remove the amplitude variation is to design a cross-talk matrix C that weighs the wavefields to even-out the amplitude effects of the encoding scheme. Presently, both the noise and amplitude variation can be addressed by increasing the number of experiments used in the production of the final image. If all possible experiments are used, then the TSV scheme approximates conventional shot-record migration. The difference between the best possible image for TSV and conventional migration is determined by the choice of the cross-talk matrix C.

One of the outstanding questions is whether or not our approximations to the identity matrix produce the best images via TSV. We chose to examine only the Gaussian and a boxcar taper approximations because they seem to be two obvious candidates. Other interesting candidates include other tapered functions such as a sinc or double-sided, decaying exponential. Further, we have not yet explored how the parameters, such as standard deviation, that control the size or length of the window affect the results. We suspect that overall these parameters control how much spatial resolution is lost during the encoding process because they control how many near wavefields are combined together to form an image. Consequently, these parameters probably influence the singular values and thus are related to the image quality at certain levels of truncation.

More research is needed on how to quantify the amount of noise that is added to the image, and on a way to quantify how much of the image is lost based on the number of experiments. By examining the quality of the image as a function of the number of experiments, one may be able to find an optimum number of simultaneous source experiments to conduct. Right now, we base the number of experiments to use on the singular values.

Additionally, we conjecture that the simultaneous source encoding framework that we have developed is independent of dimensionality, i.e. 2-D or 3-D, because the matrix representation deals solely with reconstructed wavefields based on the physical relation of shots in a large array. Therefore, the simultaneous source encoding scheme is likely applicable to three-dimensional data, as long as the spatial relationship between the sources and the encoding matrix E is maintained.

Lastly, TSV encoding is not dependent on any of the following: survey parameters, geologic structure, the velocity

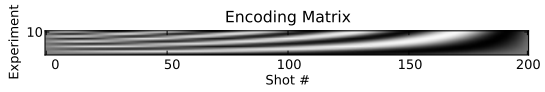

(a)

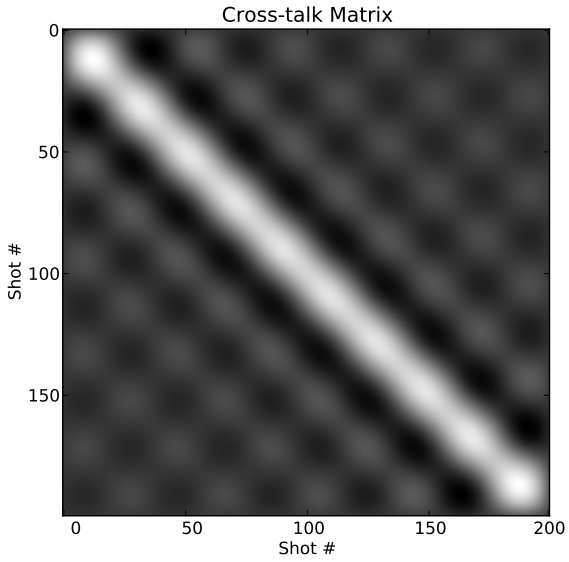

(b)

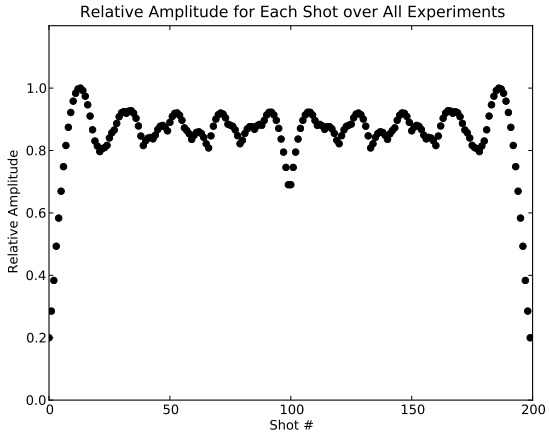

(c)

Figure 6. The transpose of the encoding matrix (a) constructed by truncating the singular vectors for a boxcar approximation for 10 simultaneous source experiments. Note the oscillatory nature of the weights in the encoding matrix. The reconstructed C matrix (b) obtained from EE^T. For both (a) and (b), white values are (1) and black values are (-1). The relative amplitudes (c) across all 10 experiments for each shot-gather. Not all shots contribute to the image equally, which means there is a spatial variation in the amplitude caused by the encoding.

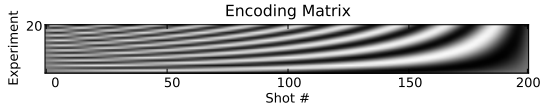

(a)

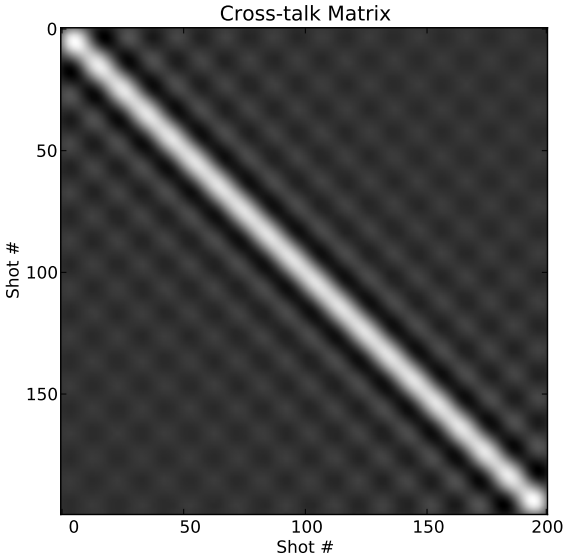

(b)

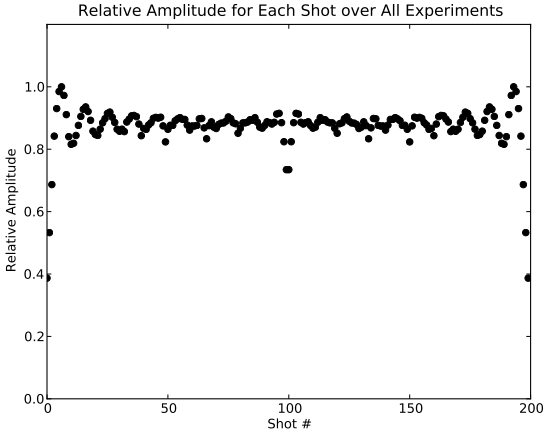

(c)

Figure 7. The transpose of the encoding matrix (a) constructed by truncating the singular vectors for a boxcar approximation. The additional experiments are more oscillatory than those in Figure 6(a). For both (a) and (b), white values are (1) and black values are (-1). There are 20 simultaneous source experiments. The reconstructed C matrix (b), obtained by multiplying EE^T. The overall amplitudes (c) across all 20 experiments for each shot-gather show less variation as a function of shot-gather than those in Figure 6(c).

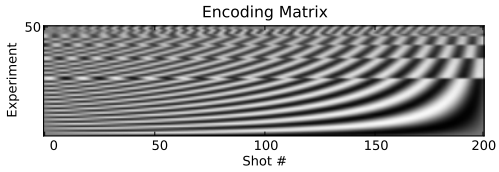

(a)

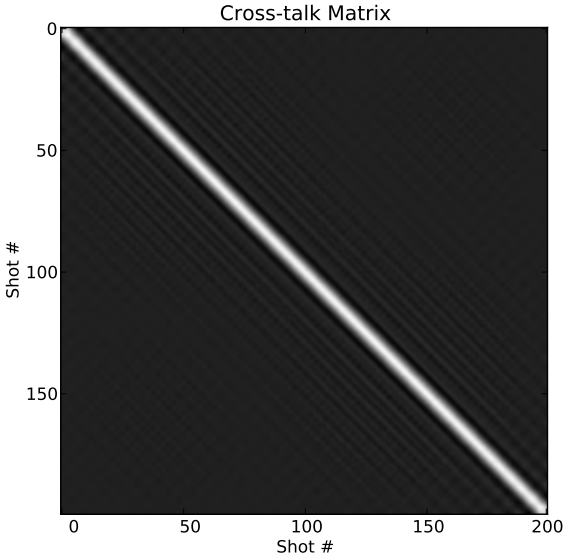

(b)

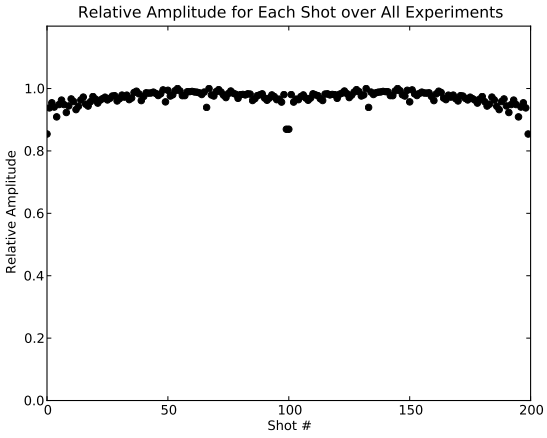

(c)

Figure 8. The transpose of the encoding matrix (a) constructed by truncating the singular vectors for a boxcar approximation. There are 50 simultaneous source experiments. The reconstructed C matrix (b), obtained by multiplying EE^T. For both (a) and (b), white values are (1) and black values are (-1). The overall amplitudes (c) across all 50 experiments for each shot-gather show that the average value of the amplitude is more closely grouped than in Figure 6(c) or Figure 7(c) which indicates that the amplitudes can be globally rescaled.

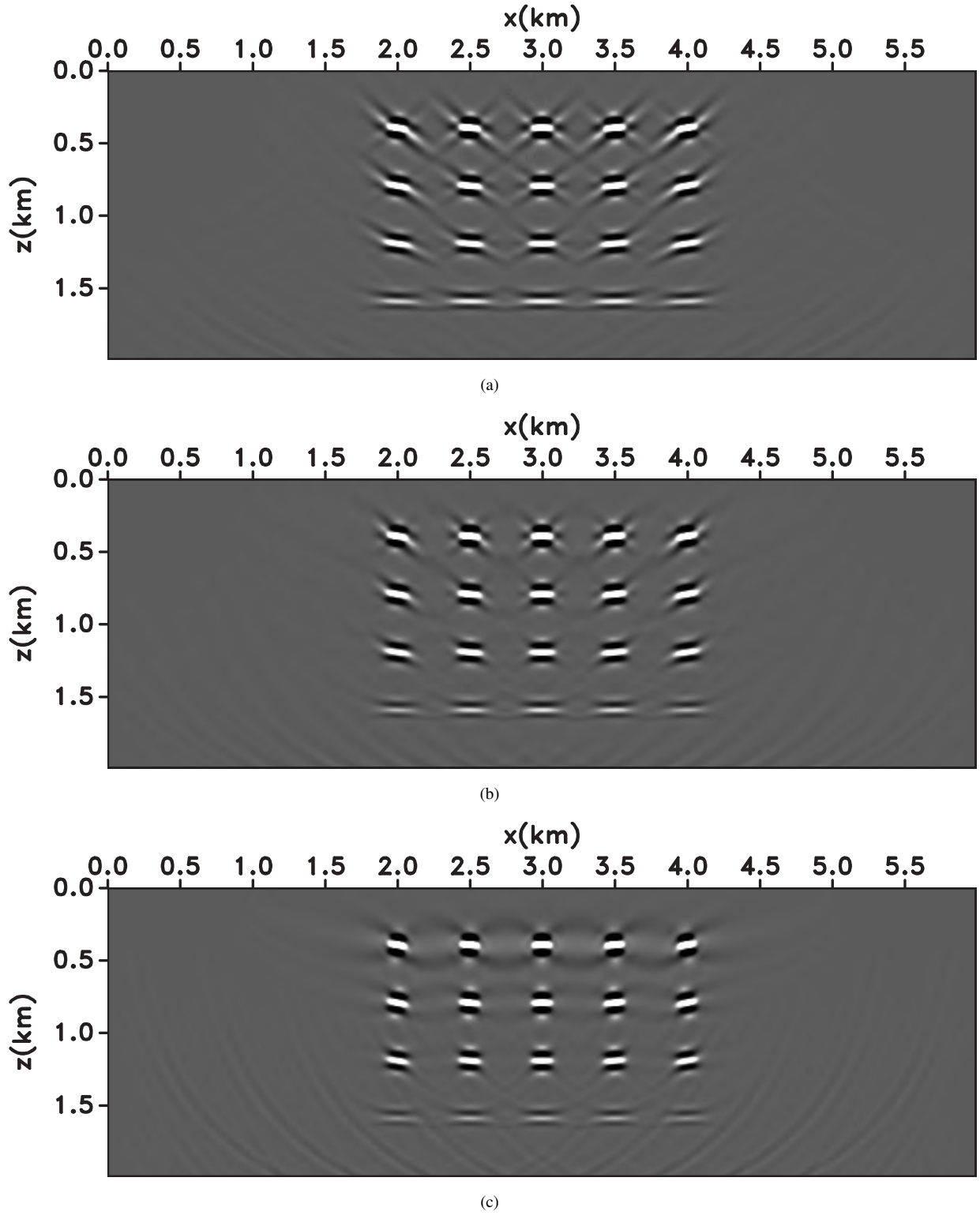

Figure 9. The final stacked images for 10 (a), 20 (b) and 50 (c) experiments using the boxcar approximation. The image quality increases as the number of experiments increases.

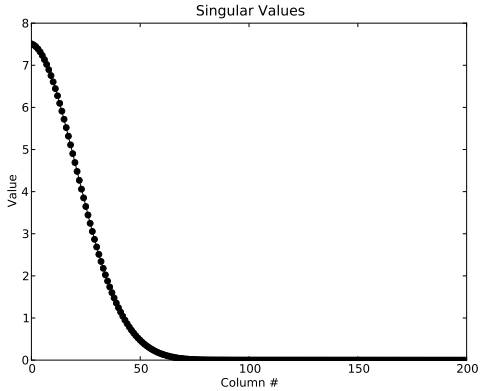

Figure 10. The singular values for the Gaussian approximation to the identity matrix for the model with point scatterers. The Gaussian distribution has a mean $\mu = 0$ and a standard deviation $\sigma = 2$.

model or migration type. The encoding scheme only depends on the number of experiments used to construct the final image, and the approximation to the identity matrix to be decomposed. Therefore, if an optimal combination of the two parameters can be found, then the cost of seismic imaging may be reduced even further.

5 CONCLUSIONS

We develop a theoretical framework that adequately explains both conventional seismic imaging and simultaneous source imaging. The framework allows us to reformulate the problem of simultaneous source imaging in the context of matrix operations and leads to the use of singular value decomposition to construct optimal encoding matrices. This allows us to identify simultaneous source encoding schemes, such as Truncated Singular Vector (TSV), that produce migrated images at much lower cost than conventional shot-record migration. The encoded migrations trade reduced computational cost with increased noise in the image, spatial amplitude variation, and loss of spatial resolution. We demonstrate the validity of these encodings through numerical experiments on both a simple model and on the geologically complex Sigsbee2A salt model. In both cases, the Truncated Singular Vector encoding scheme reduces the cost of imaging by at least an order of magnitude while restricting cross-talk noise and maintaining spatial resolution.

6 ACKNOWLEDGMENTS

We would like to thank Francesco Perrone for many enlightening conversations on this subject, as well as technical support. The reproducible numeric examples in this paper use the Madagascar open-source software package freely available from http://www.reproducibility.org. This research was supported in part by the Golden Energy Computing Organization at the Colorado School of Mines using resources acquired with financial assistance from the National Science Foundation and the National Renewable Energy Laboratory.

REFERENCES

Akerberg, P., Hampson, G., Rickett, J., Martin, H., and Cole, J., 2008, Simultaneous source separation by sparse radon transform: SEG Technical Program Expanded Abstracts, **27**, no. 1, 2801.

Beasley, C. J., 2008, A new look at marine simultaneous sources: The Leading Edge, **27**, no. 7, 914.

Berkhout, A. J. G., Blacquiere, G., and Verschuur, E., 2008, From simultaneous shooting to blended acquisition: SEG Technical Program Expanded Abstracts, **27**, no. 1, 2831.

Berkhout, A., Verschuur, D., and Blacquiere, G., 2009, Seismic imaging with incoherent wavefields: Seismic imaging with incoherent wavefields:, SEG Technical Program Expanded Abstracts, 2894–2898.

Blacquiere, G., Berkhout, G., and Verschuur, E., 2009, Survey design for blended acquisition: Survey design for blended acquisition:, SEG Technical Program Expanded Abstracts, 56–60.

Eckart, C., and Young, G., 1936, The approximation of one matrix by another of lower rank: Psychometrika, **1**, no. 3, 211–218.

Hampson, G., Stefani, J., and Herkenhoff, F., 2008, Acquisition using simultaneous sources: The Leading Edge, **27**, no. 7, 918.

Huo, S., Luo, Y., and Kelamis, P., 2009, Simultaneous sources separation via multi-directional vector-median filter: Simultaneous sources separation via multi-directional vector-median filter:, SEG Technical Program Expanded Abstracts, 31–35.

Kim, Y., Gruzinov, I., Guo, M., and Sen, S., 2009, Source separation of simultaneous source OBC data: Source separation of simultaneous source OBC data:, SEG Technical Program Expanded Abstracts, 51–55.

Liu, F., 1999, Plane wave source composition: An accurate

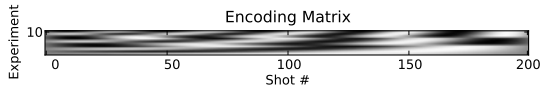

(a)

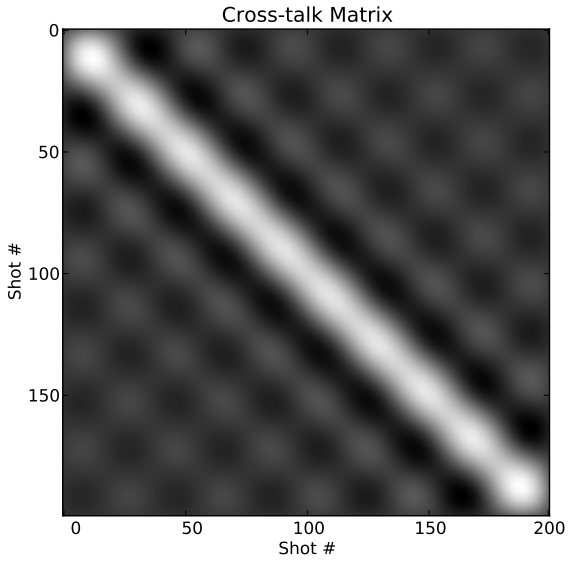

(b)

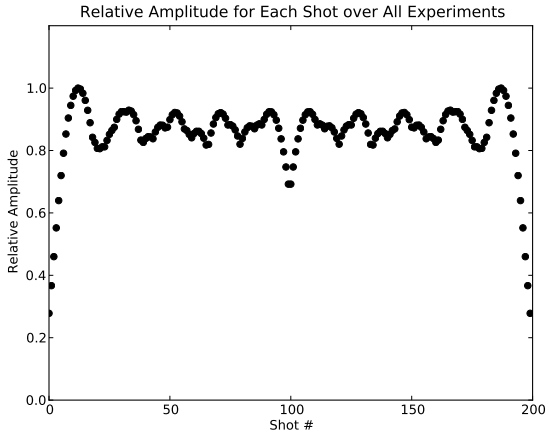

(c)

Figure 11. The transpose of the encoding matrix (a) constructed by truncating the singular vectors for a Gaussian approximation. There are 10 simultaneous source experiments, which means the K is 20. The reconstructed C matrix (b), obtained by multiplying EE^T. In (a) and (b), white values are (+1) and black values are (-1). The overall amplitudes (c) across all 10 experiments for each shot-gather. There is an amplitude variation as a function of shot, so the amplitudes in the final image are spatially variable due to the encoding.

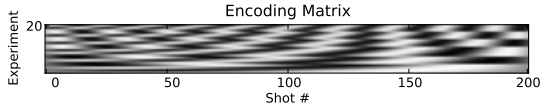

(a)

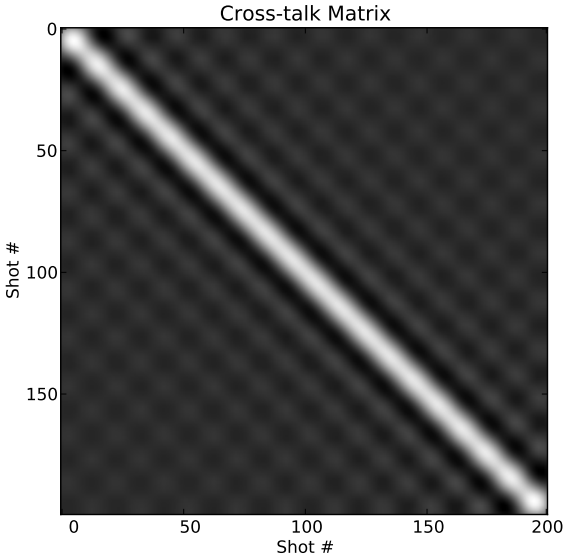

(b)

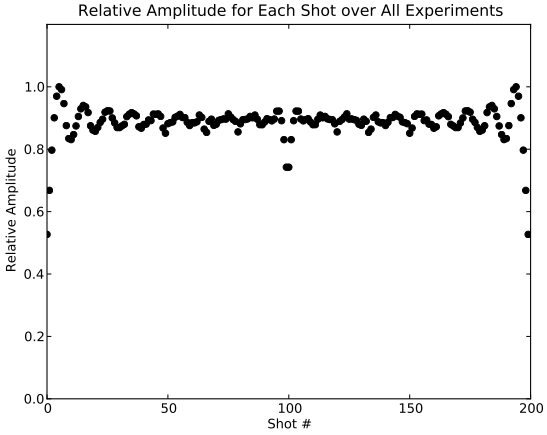

(c)

Figure 12. The transpose of the encoding matrix (a) constructed by truncating the singular vectors for a Gaussian approximation. There are 20 simultaneous source experiments or $K = 10$. The reconstructed C matrix (b), obtained by multiplying EE^T. In (a) and (b), white values are (+1) and black values are (-1). The overall amplitudes (c) across all 20 experiments for each shot-gather. The amplitude variation as a function of shot is identical to the variation for the boxcar, Figure 7(c).

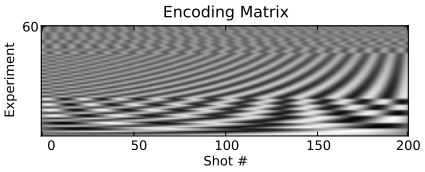

(a)

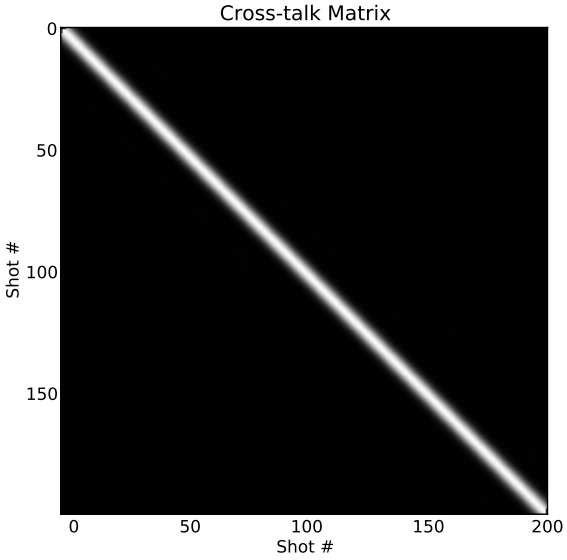

(b)

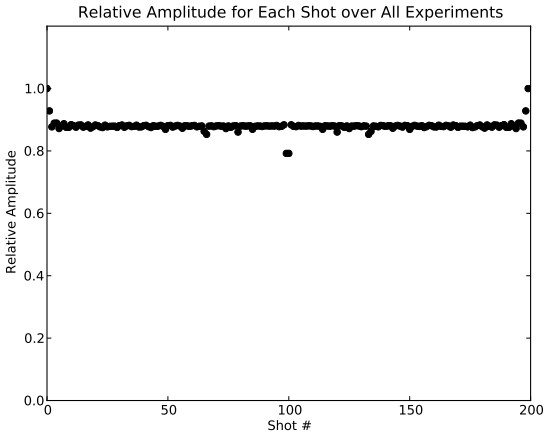

(c)

Figure 13. The transpose of the encoding matrix (a) constructed by truncating the singular vectors for a Gaussian approximation. There are 60 simultaneous source experiments. The reconstructed C matrix, obtained by multiplying EE^T (b). In (a) and (b), white values are (+1) and black values are (-1). The overall amplitudes (c) across all 60 experiments for each shot-gather. The spatial amplitude variation is more consistent in this case, which indicates that the amplitudes can be globally rescaled to match the conventional image's amplitudes.

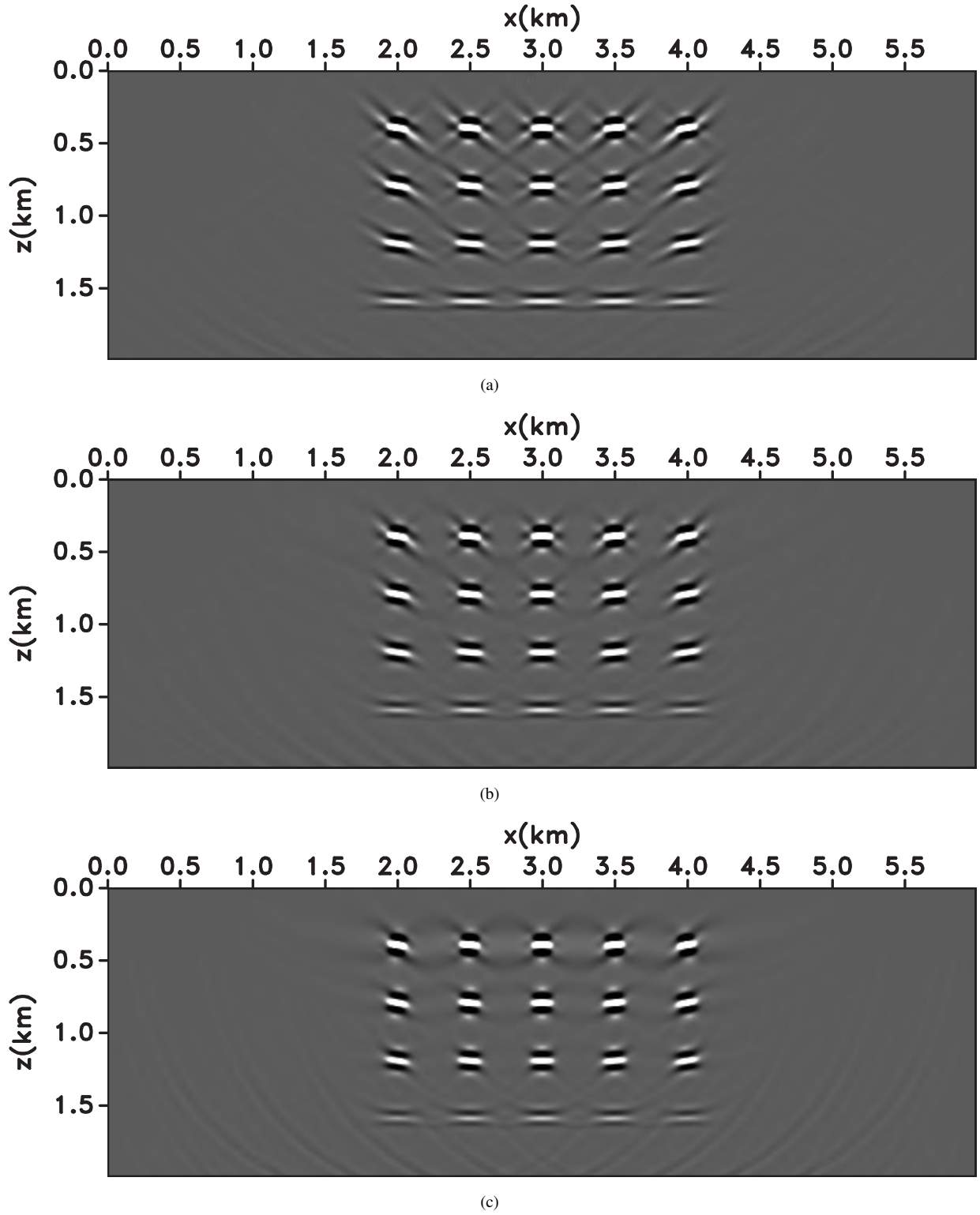

(a)

(b)

(c)

Figure 14. The final stacked image (a) for 10 experiments. The stacked image (b) for 20 experiments and the stacked image (c) for 60 experiments. All experiments used the Gaussian filter as the cross-talk C matrix. The image quality increases as the number of experiments increases.

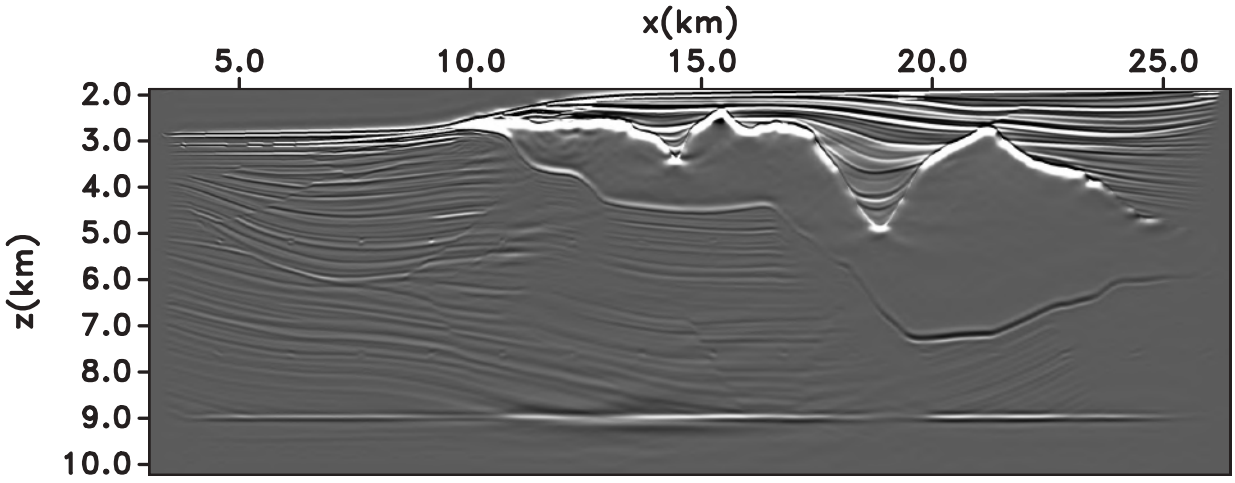

Figure 15. The stacked image of Sigsbee using conventional shot-record migration for all 3200 shots.

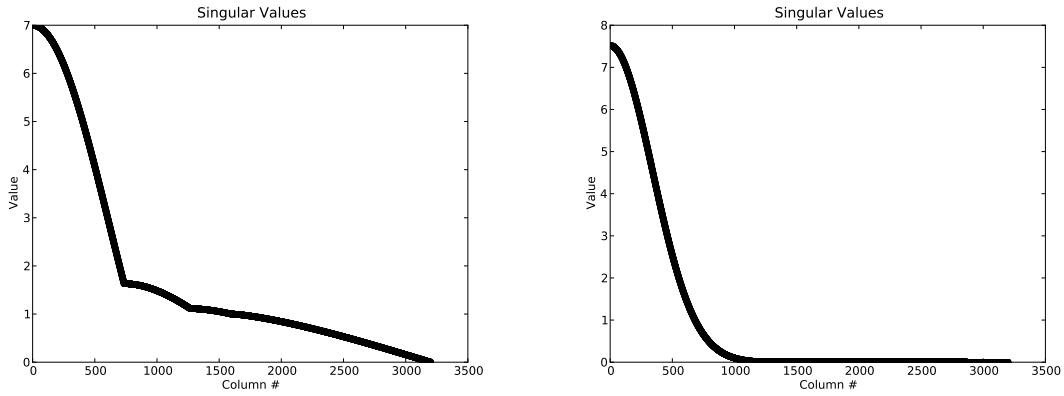

(a) (b)

Figure 16. The singular values for the Sigsbee survey using the boxcar approximation (a) and the Gaussian approximation (b).

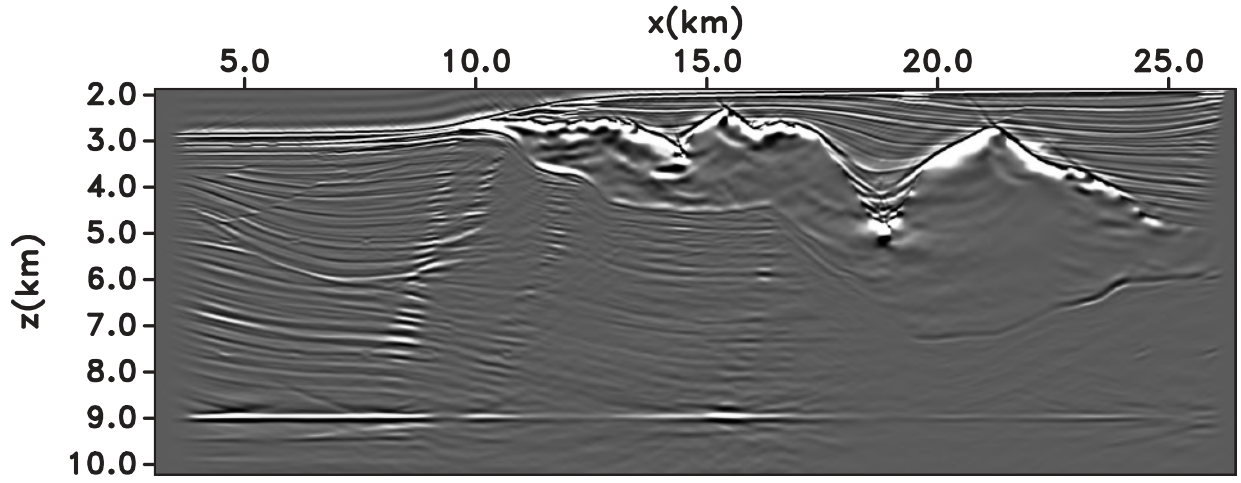

(a)

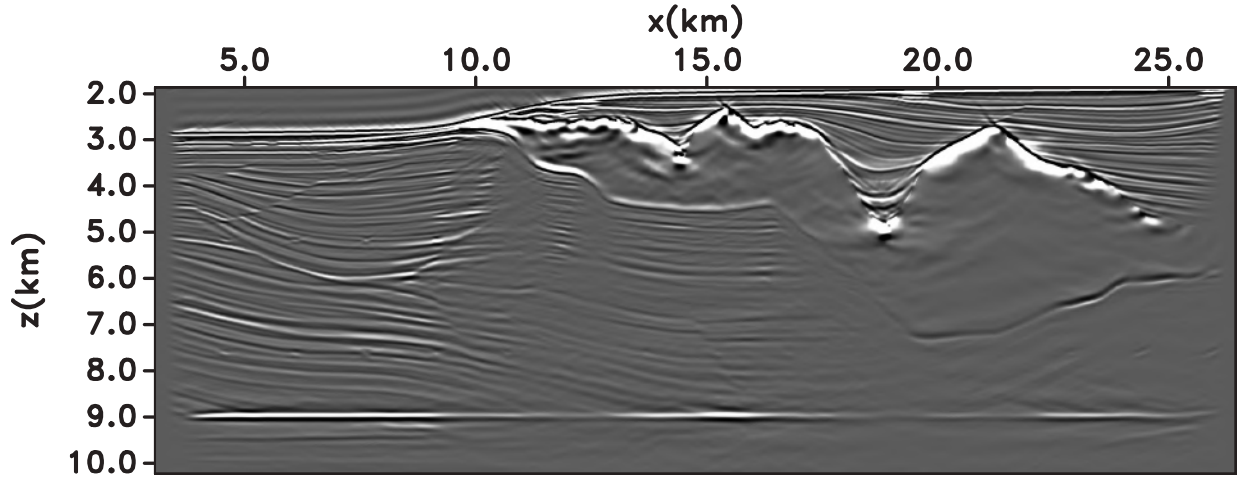

(b)

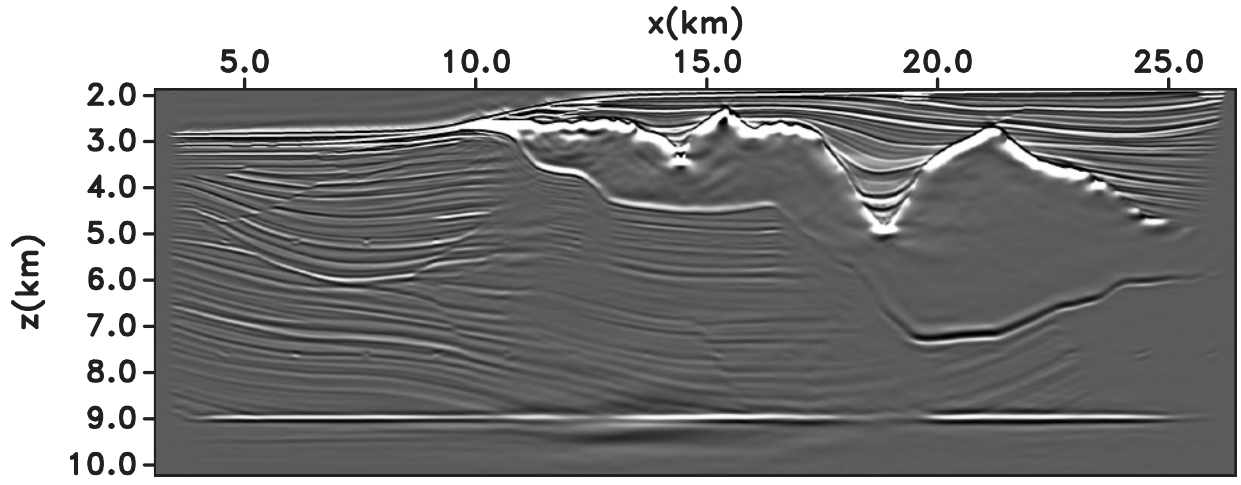

(c)

Figure 17. The image of Sigsbee using the Gaussian approximation for 10 experiments (a), 30 experiments (b), and 100 experiments (c). While (a) and (b) cost significantly less than (c), the image quality in (c) is much better than that of the images shown in (a) and (b) when compared against Figure 15.

phase encoding scheme for prestack migration: SEG Technical Program Expanded Abstracts, **21**, no. 1, 1156.

Morton, S. A., 1999, Fastershot-record depth migrations using phase encoding: SEG Technical Program Expanded Abstracts, **17**, no. 1, 1131.

Perrone, F., and Sava, P., 2009, Comparison of shot encoding functions for reverse-time migration: Comparison of shot encoding functions for reverse-time migration:, SEG Technical Program Expanded Abstracts, 2980–2984.

Rabbani, M., 1991, Digital image compression techniques: , Spie Optical Engineering Press, Bellingham Wash. USA.

Romero, L. A., Ghiglia, D. C., Ober, C. C., and Morton, S. A., 2000, Phase encoding of shot records in prestack migration: Geophysics, **65**, no. 2, 426.

Salomon, D., 2007, Data compression : the complete reference: , Springer, London, 4th ed. edition.

Soubaras, R., 2006, Modulated-shot migration: SEG Technical Program Expanded Abstracts, **25**, no. 1, 2430.

Spitz, S., Hampson, G., and Pica, A., 2008, Simultaneous source separation: A prediction-subtraction approach: SEG Technical Program Expanded Abstracts, **27**, no. 1, 2811.

Ting, C., and Zhao, W., 2009, A simulated wide azimuth simultaneous shooting experiment: A simulated wide azimuth simultaneous shooting experiment:, SEG Technical Program Expanded Abstracts, 76–80.

Womack, J. E., 1990, Encoding techniques for multiple source point seismic data acquisition: Geophysics, **55**, no. 10, 1389.

Zhang, Y., Sun, J., and Gray, S., 2007, Reverse-time migration: Amplitude and implementation issues: SEG Technical Program Expanded Abstracts, **26**, no. 1, 2145.